Neuronal inclusions of α-synuclein contribute to the pathogenesis of Krabbe disease

Benjamin R. Smith[1,2], **Marta B. Santos**[1,2], **Michael S. Marshall**[1,2], **Ludovico Cantuti-Castelvetri**[1], **Aurora Lopez-Rosas**[1], **Guanan Li**[3], **Richard van Breemen**[3], **Kumiko I. Claycomb**[4], **Jose I. Gallea**[5], **Soledad M. Celej**[5], **Stephen Crocker**[4], **Maria I. Givogri**[1], and **Ernesto R. Bongarzone**[1,*]

[1]Department of Anatomy and Cell Biology, College of Medicine, University of Illinois, University of Illinois Chicago, Chicago Il 60612

[3]Department of Medicinal Chemistry and Pharmacognosy, College of Pharmacy, University of Illinois, University of Illinois Chicago, Chicago Il 60612

[4]Department of Neuroscience, University of Connecticut Health Center, Farmington, CT

[5]Departamento de Quimica Biologica, CIQUIBIC, CONICET, Universidad Nacional de Cordoba, Cordoba, Argentina

Abstract

Demyelination is a major contributor to the general decay of neural functions in children with Krabbe disease. However, recent reports have indicated a significant involvement of neurons and axons in the neuropathology of the disease. In this study, we have investigated the nature of cellular inclusions in the Krabbe brain. Brain samples from the Twitcher mouse model for Krabbe disease and from patients affected with the infantile and late onset forms of the disease were examined for the presence of neuronal inclusions. Our experiments demonstrated the presence of cytoplasmic aggregates of thioflavin-S reactive material in both human and murine mutant brains. Most of these inclusions were associated with neurons. A few inclusions were detected to be associated with microglia and none were associated with astrocytes or oligodendrocytes. Thioflavin-S reactive inclusions increased in abundance paralleling the development of neurological symptoms and distributed throughout the Twitcher brain in areas of major involvement in cognition and motor functions. Electron microscopy confirmed the presence of aggregates of stereotypic β-sheet folded proteinaceous material. Immunochemical analyses identified the presence of aggregated forms of α-synuclein and ubiquitin, proteins involved in the formation of Lewy bodies in Parkinson's disease and other neurodegenerative conditions. In vitro assays demonstrated that psychosine, the neurotoxic sphingolipid accumulated in Krabbe disease, accelerated the fibrillization of α-synuclein. This study demonstrates the occurrence of neuronal deposits of fibrillized proteins including α-synuclein, identifying Krabbe disease as a new α-synucleinopathy.

*Correspondence: Ernesto R. Bongarzone, Department of Anatomy and Cell Biology, College of Medicine, University of Illinois at Chicago, 808 South Wood St., MC512, Chicago, IL 60612. Telephone: 312-996-6894 Fax: 312-413-0354 ebongarz@uic.edu.
[2]These authors contributed equally to this work

Keywords

Krabbe disease; myelin; psychosine; dying-back pathology; axonal degeneration; synucleinopathies; α-synuclein; ubiquitin; Lewy bodies

Introduction

Brain inclusions of misfolded proteins develop in Sandhoff and Tay-Sachs lysosomal storage diseases (LSDs) [1]. The functional significance of these deposits and the extent to which they occur in other LSDs is unclear. Krabbe disease is caused by over a hundred different mutations in the β-galactosylceramidase (GALC) gene [2] and the subsequent deficient lysosomal degradation of galactosylsphingolipids. Affected patients develop progressive demyelination, cognitive and developmental deficiencies and die very young. These neuropathological features are largely caused by the accumulation of undegraded psychosine[3–6]Psychosine is a lipid raft-associated neurotoxin, affecting a number of cellular functions that lead to demyelination, oligodendrocyte death, axonal degeneration, inhibition of axonal transport [3,7–17]. Patients suffer from muscle rigidity and atrophy, ataxia, and neuronal deficits [17–20], suggesting the presence of brain lesions affecting major neuronal pathways. The pathogenic mechanism causing this neuronal dysfunction is still unclear, but it appears to involve at least defects on fast axonal transport and on the neuronal cytoskeleton [17,21]. Much of the research on Krabbe has been performed on the naturally occurring Twitcher murine model, an enzymatically equivalent model of Krabbe disease [22]. Twitcher mice carry a single mutation that abolishes the lysosomal activity of GalC [23,24]. Inclusions of electron dense material have been reported in the Twitcher brain but the chemical composition and relevance of these inclusions remained unaddressed.

α-Synuclein is a soluble protein of unknown function, primarily localized at the presynaptic terminus of central axons [25,26]. Deposits of fibrillizated α-synuclein and other proteins such as ubiquitin have been associated with neurological defects in α-synucleinopathies, which include Parkinson's disease, dementia with Lewy bodies, multiple system atrophy (MSA), some variants of Alzheimer's disease [27–32] and recently some LSDs [1]. How α-synuclein leads to neuropathology is unclear but it may involve abnormal gain-of-function signaling initiated by intermediate α-synuclein oligomers formed during the process of fibrillization [33–35]. Fibrillization involves the formation of intermediate α-synuclein oligomers [36], which are more toxic than the mature fibrils [37–40]. Several mutations increase the rate of fibrillization of α-synuclein [41–47]. However, for the most part, the molecular mechanism of fibrillization of α-synuclein in vivo is still unknown.

Here, we investigated the hypothesis that Krabbe disease, as seen in other LSDs, is compounded by neuronal inclusions of misfolded protein aggregates. Our experiments identified neuronal inclusions in both the human and murine Krabbe brain, revealing these protein inclusions to consist primarily of aggregated α-synuclein, increase in frequency during disease, and affect specific brain areas. Furthermore, psychosine was found to facilitate α-synuclein fibrillization.

Materials and Methods

Animals and human tissue

Twitcher mice were identified by PCR [23]. Frontal cortex specimens from infants affected by Krabbe disease, Parkinson's disease and age-matched control tissue were obtained from the National Institutes of Health Brain Tissue bank at University of Maryland (cases 575, 5100 and 4247) and from the Harvard Brain bank (case 1414). Animal and human work in

this study was performed under approved protocols from the Animal Care Committee (Protocol 12–123) and the Office for Protection of Human Subjects (Protocol # 2011-0515) at the University of Illinois at Chicago.

Thioflavin-S staining

Free-floating brain tissue slices were washed with TBS, mounted onto slides, air-dried and then rehydrated with ultrapure water. Sections were stained with 0.1% Thioflavin-S ethanol/PBS for 5 minutes, rinsed in 80% ethanol for 5 minutes and mounted using Vectashield (Vector laboratories).

Fibrillization assay

Recombinant synuclein was dissolved in α-synuclein was dissolved in PBS and filtered through a 0.22μm filter to yield 0.5mg/ml. Thioflavin T (Sigma) was dissolved in ultrapure water at 0.3% w/v. Psychosine (Matreya) was dissolved in ethanol. Fifteen micrograms of α-synuclein was dispensed in 1 ml of PBS in the presence of psychosine at final concentrations ranging from 0.01 μM to 1μM or vehicle (0.005% ethanol/PBS) in dark glass bottles. Solutions were shaken at 37°C at 600rpm. Fifty microliter aliquots (in triplicates) were removed at different time points and loaded onto black 96 well plates and mixed with 5 μL of Thioflavin-T stock solution. Samples were analyzed using a DTX880 Spectrometer (Beckman) at 450/535 nm excitation/emission. Additionally, 3 μL from each experimental condition was processed for transmission electron microscopy as described below.

Transmission electron microscopy

Tissue was fixed with 2.5% glutaraldehyde, and embedded in Araldite. Ultrathin sections (60-nm) were processed for transmission electron microscopy (TEM). Aliquots (3 μL) from each fibrillization condition were transferred onto carbon-coated 400 mesh nickel grids. Grids were negatively stained with 2% w/v uranyl acetate. Immunoelectron microscopy was performed on 100 μm thick sections using free floating penetration of primary antibodies followed by Aurion (0.8 nm) gold-secondary antibodies. Sections were post-processed for TEM as described above. Grids were viewed using a 120kV JEOL JEM-1220 equipped with a Gatan Es1000W 11MP CCD camera.

Stereology

Sagittal brain sections (50-micron) (one every 10 sections) were stained with thioflavin-S. Thioflavin-S positive inclusions were quantified from 6 sections using the design-based stereology system (StereoInvestigator version 8, MBF Bioscience, Williston, VT, USA). Briefly, the caudate putamen was traced under a 5× objective and thioflavin-S positive cells were counted under a 63× objective. Sampling parameters were set up for the coefficient of error to range between 0.09 and 0.12 using the Gundersen test, normally with a counting frame size of 100×100 micron, optical dissector height of 20 microns, and an average of 10 sampling sites per section.

Extraction protocol and western blotting

Tissue was homogenized in 15 volumes of 1mM PMSF, 2mM sodium orthovanadate, 1mM NaF and 300nM okadaic acid in TBS. Samples were centrifuged at 100,000g at 4°C for 1 hour. The TBS soluble supernatant was removed and kept frozen. The pellet was resuspended in 15 volumes (w/v) TBS with 1% Triton-X 100 (TBS-X) and rotated for 30 minutes at 4°C before centrifugation at 100,000 g at 4°C for 1 hour. The supernatant was removed and frozen. The pellet was resuspended in 400μL of 70% formic acid and rotated for 1 hour before neutralization by the addition of 20 volumes of 1M Tris. Protein extracts were separated by SDS-PAGE and electrotransferred onto PVDF membranes. Blots were

incubated with primary antibodies at 4°C overnight. The following antibodies were used: monoclonal antibody against α-synuclein cat#610786 (BD Biosciences, 1:1000 dilution), polyclonal antibody A11 cat# AHB0052 (Invitrogen, 1:1000 dilution), and monoclonal antibody against actin cat# A2066 (Sigma, 1:6000 dilution). Immunocomplexes were visualized using enhanced luminescence (Thermo Sci.).

Real Time-Polymerase Chain Reaction

RNA was extracted using Trizol. Two micrograms of RNA was used for synthesis of cDNA (Invitrogen). The amplification cycle was monitored with SYBR-490 and the mRNA expression level was deduced from the fold differences between control and sample and differences within each sample group. Primers were designed with NCBI and verified by mFold software tools. α-Synuclein primers were: Forward, 5′-AGCAGTGGTGACGGGTGT and Reverse, 5′-GGGCTCCTTCTTCATTCTTGCC; GAPDH, Forward 5′-GAGTCAACGGATTT GGTCGTA and Reverse 5′-CCATGTAGTTGAGGTCAATGAAGG.

Immunohistochemistry

Mice were anesthetized and perfused with saline followed by 4% paraformaldehyde and processed for cryosectioning. Cryosections (20 micron) were incubated with monoclonal antibodies against α-synuclein cat#2628 (Cell Signaling, 1:100 dilution), proteolipid protein (AA3 1:10 dilution), GFAP cat#Ab9598 (Millipore 1:500 dilution), and Amyloid Beta (MOAB-2) cat#M-1586-100 (Biosensis 1:500 dilution). Immunofluorescent-complexes were visualized using a Zeiss Meta 510 confocal microscope. Some experiments were developed using the peroxidase-diamino-benzidine (DAB) method and imaged using a DM5500 Q Microscope with a Leica DFC 500 Camera.

Psychosine determination

Psychosine was quantified as detailed elsewhere [48]. Briefly, after extraction with chloroform and methanol and fractionation on a cation exchanger column, samples were analyzed by liquid chromatography tandem mass spectrometry (LC-MS/MS) using a Shimadzu LC-10Advp. Positive ion electrospray tandem mass spectrometry was performed using an Applied Biosystems (Foster City, CA) API 4000 triple quadrupole mass spectrometer with a collision energy of 29 eV for psychosine and 37 eV for the internal standard, lyso-lactosylceramide.

Statistical Analysis

Data was analyzed using ANOVA assuming non-gaussian distributions. p-Values <0.05 were considered significant. Graphs represent the mean of independent measurements (with sample size between 3–6) and ± SEM.

Results

Anatomical and temporal distribution of protein aggregates in the Twitcher mouse

Thioflavin-S positive inclusions were detected in the Twitcher brain (Figure 1) throughout the postnatal life. The first detectable inclusions appeared in the pontine region (pons) at P10 (Figure 1A, inset). At P20, two other foci were detected in the pontine grey area (Fig. 1B, #1) and the superior olivary complex (Fig. 1B, #2). Inclusions were also detected throughout the medulla (Fig. 1B, #3) and the spinal nucleus of the trigeminal nerve (Fig. 1B, #4). Inclusions were abundant in the midbrain region (Fig. 1B, #5), substantia nigra (Fig. 1B, #6), the reticular nucleus (Fig. 1B, #7), the inferior region of the superior colliculus (Fig. 1B, #9), the inferior colliculus (Fig. 1B, #10), hypothalamus (Fig. 1B, #11) and caudate putamen

(Fig. 1B, #12). Inclusions were also present in the rostral portions of the nucleus accumbens (Fig. 1B, #13), the olfactory tubercle (Fig. 1B, #14), internal granular layer in the cerebellum (Fig 1B, #16) and the CA2 region of the hippocampus (Fig. 1B, #15). At this postnatal age, the Twitcher cerebral cortex was essentially devoid of inclusions.

At P30, inclusions were detected spreading caudally and ventrally in the caudate putamen region (Fig. 1C, #12), engulfing the nucleus accumbens (Fig. 1C, #13). More inclusions were evident in the lateral pre-optic area of the hypothalamus (Fig. 1C, #17), the optic tract, superior red nucleus (Fig. 1C, #18), the superior colliculus (Fig. 1C, #9), rostral areas of the thalamus including the lateral dorsal nucleus (Fig. 1C, #19a), anteroventral nucleus (Fig. 1C, #19b) and the reticular nucleus (Fig. 1C, #19c). Inclusions were detected throughout the cerebellar arbor vitae (Fig. 1C, #20), the vestibular nuclei (Fig. 1C, #21) and more scarcely, in the posterior regions of cortical layer 1 (Fig. 1C, #22).

The P40 Twitcher brain developed additional inclusions within the cerebellar cortex (Fig. 1D, #16), posterior regions of layers 1 (Fig. 1D, #22), 3/4 (Fig. 1D, #23), and 6b (Fig. 1D, #24) (along the corpus callosum). Deposits in these layers were primarily localized to the retrosplenial, anterior cingulate and somatomotor areas of the cerebral cortex, yet were noticeably fewer in the frontal cortex (Fig. 1D, #25). Inclusions were also abundant in the thalamus (Fig. 1D, #19). In addition to inclusions within the CA2 region, aggregates were also detected in the subiculum (Fig. 1D, #26) and dentate gyrus (Fig. 1D, #27). Magnified images (5× and 63×) depicting inclusions in multiple anatomical regions of the P40 Twitcher are shown in Figure 2. Wild type brains were devoid of any thioflavin-S positive inclusions (Fig. 1E, Fig. 2) at any time point, as well as mice heterozygous for the mutation (Sup. Fig. 1). Unstained, fresh P40 Twitcher brain tissue (Fig. 1F, H) was imaged under a 480nm filter to detect the presence of autofluorescent material (such as accumulated lipofucsin) that was non-specific to thioflavin-S staining. The unstained area imaged was recorded and the same location was re-imaged after subsequent thioflavin-S staining (Fig. 1G, I). Autofluorescent deposits were rarely seen in Twitcher tissue (arrowheads) compared to the abundant deposits of thioflavin-S reactive material (arrows). Positive control of autofluorescent lipofucsin deposits is shown in aged human cortex (Fig. 1J, K), which also contained sporadic thioflavin-S reactive deposits. Changes in the density of thioflavin-S positive inclusions during the progression of the disease were evident in the Twitcher brain. Stereology inclusions within the caudate putamen showed significant increases at each time point from P20 to P30 ($p=0.001-0.005$) to P40 ($p=0.002$) (Fig. 2).

Thioflavin-S inclusions are predominantly neuronal

Thioflavin-S stained brain slices were co-immunolabeled to visualize neurons, astrocytes, oligodendrocytes and microglia. Thioflavin-S inclusions were not detected in GFAP positive astrocytes (Fig. 3E, F) or APC positive oligodendrocytes (data not-shown). In contrast, thioflavin-S inclusions almost exclusively co-localized with NeuN positive neurons (Fig. 3A, B) and occasionally in isolectin IB4 positive cells (Fig. 3C, D), suggesting that some inclusions either form in activated microglia or are engulfed by these cells.

Ultrastructure of neuronal protein aggregates

TEM identified neuronal aggregates in Twitcher brains at P40, which ranged in density, shape and size (arrows in Fig. 3J). These were never detected in wild-type brains (Fig. 3I). Intracellular deposits surrounded by membranes were frequent (Fig. 3K). A closer examination of these membrane-bound inclusions showed the presence of abundant ~5nm wide electron dense spheroid material, (asterisk in Fig. 3L). In some cases, these spheroids appeared to form large concatenated tubular structures ranging from 200 to 400nm in length (arrowheads in Fig. 3L). In addition, aggregates devoid of membrane were also detected

(Fig. 3M). These structures appeared as electron dense fibrils of approximately 100 to 150nm in width and up to 700 nm in length (Fig, 3N–P), bearing the stereotypic structure of fibrils seen in Parkinson's and Alzheimer's diseases.

α-Synuclein and ubiquitin are components of Krabbe inclusions

Immunohistochemistry using a panel of specific antibodies was performed to identify the protein components of the inclusions detected in the Twitcher brain. Figure 4A–E shows confocal images taken from P40 Twitcher brain sections double labeled for thioflavin-S and α-synuclein. Orthogonal views from z-stack confocal analyses showed strong co-localization of α-synuclein within the core of thioflavin-S positive inclusions. Co-localization of α-synuclein in thioflavin-S was observed at all time points from P10 to P40 (data not-shown). α-Synuclein inclusions were not found in either wild-type or heterozygous twitcher (Supplementary Fig. 2). Immunoelectron microscopy further confirmed the association of α-synuclein immunoreactivity with inclusions observed in Twitcher neurons (Fig. 3F and inset). Specificity of the anti-α-synuclein antibody was confirmed using immunohistochemistry on brain tissue from α-synuclein knockout mice (SCNA KO) (Supplementary Fig. 2). The presence of α-synuclein positive aggregates in the Twitcher brain was not associated with gross changes in expression of α-synuclein mRNA (Fig. 3H) or protein (Fig. 3I). In addition to α-synuclein, ubiquitin was also found to be associated with most thioflavin-S positive inclusions (Supplementary Fig. 3A, B). We were unable to detect the presence of other neurological protein markers such as β-amyloid (Supplementary Fig. 2) or amyloid precursor protein (data not-shown).

α-Synuclein inclusions in the brain of Krabbe patients

To determine whether similar inclusions affect the brain of human Krabbe patients, brain sections from three available infantile Krabbe cases were stained with thioflavin-S (Fig. 5A–F). Figure 5A–C shows the presence of numerous thioflavin-S positive inclusions in grey areas from frontal lobe samples in the three infantile cases. There was a disparity in the abundance of thioflavin-S reactive material in human samples, with inclusions very abundant in all infantile onset cases. At higher magnification, the majority of inclusions appeared as amorphous aggregates (Fig. 5D). In addition, other deposits appeared as filamentous arrays of aggregated material (Fig. 5E and inset magnified in 5F). Unfortunately, the limited availability of human material from Krabbe disease patients prevented any stereological analysis of the regional distribution of inclusions. Most thioflavin-S reactive inclusions co-stained positively with antibodies against α-synuclein (Fig. 5H, I). Control tissues from healthy age-matched brains were devoid of any detectable thioflavin-S positive inclusions (Fig. 5G).

Detection of high molecular weight aggregates of α-synuclein in the Krabbe brain

We studied whether the Krabbe inclusions were accompanied by changes in the expression level, solubility and aggregation of α-synuclein. TBS, TBS-triton X-100 (TBS-X), and Formic Acid extracts [49] were prepared from basal ganglia samples from two Krabbe infant cases, the age-matched control, a Parkinson's disease case as a positive control of α-synuclein aggregates [50], and tissue from a SNCA KO mouse as a negative control. A detectable level of α-synuclein extracted more efficiently in TBS-X and FA fractions from the Krabbe samples (Fig. 5L), suggesting a decrease in solubility of this protein in the Krabbe brain. Increased levels of high molecular weight species of α-synuclein were detected in both Krabbe samples, similar to that seen in the Parkinson's case, suggesting an accumulation of aggregated *α*-synuclein protein. Using the antibody A11, which detects oligomeric forms of amyloid protein but does not react with monomeric or mature fibril amyloid forms [51], we confirmed the presence of A11 immunoreactive material in neuronal

inclusions from caudate neurons in the P40 Twitcher brain (Supplementary Fig. 4A) and of immunoreactive bands primarily in TBS extracts in both Krabbe cases (Supplementary Fig. 4C).

Inclusions are more abundant in areas rich in psychosine

To determine the extent of co-localization of thioflavin-S inclusions with psychosine accumulation, P40 Twitcher brains were microdissected and the local levels of psychosine were determined by LC-MS-MS. Table I shows psychosine elevated in all brain regions in Twitcher mice. Importantly, brain areas containing the most thioflavin-S positive aggregates also accumulated the highest levels of psychosine. For example, the caudate putamen and most of the midbrain contained the highest levels of psychosine and also the highest density of inclusions (Fig. 1D). Of interest, areas such as the cortex that contained the lowest levels of psychosine also contained the lowest density of inclusions (Fig. 1D).

Psychosine induces fibrilization of α-synuclein in vitro

To test whether or not psychosine affects α-synuclein aggregation, in vitro fibrillation assays using 0.01 to 1μM psychosine and pure recombinant human α-synuclein were conducted. Fibrillization was measured by changes in the fluorescent emission of thioflavin-T. α-Synuclein incubated with increasing concentrations of psychosine produced significantly more fluorescence than vehicle-treated α-synuclein 96 hours after initiation of shaking (Fig. 6A, B), suggesting that psychosine may facilitate the rate of fibrillization of α-synuclein in a dose-dependent manner. Psychosine did not have any fibrillization effect on β- and γ-synuclein (Fig. 6B). Fibrillized α-synuclein was analyzed by gel separation 4 days after incubation, showing a dose-dependent increase of high molecular weight bands of aggregated protein in the presence of increasing concentrations of psychosine (Fig. 6C). Similar albeit less intense bands were detected in vehicle treated conditions but at later time points (7 days, Fig. 6C).

Ultrastructural TEM studies showed the presence of large filamentous α-synuclein structures after 48 hours of shaking in the presence of 0.5 μM psychosine (Fig. 6D). These structures developed into even larger aggregates after 4 days of incubation (Fig. 6E, 6F). In comparison, vehicle-treated α-synuclein showed filamentous structures of noticeably smaller size and abundance at either time point.

Discussion

In 1916, Knud Krabbe provided the first clinical description of children affected with a diffuse form of myelin sclerosis [20]. Over decades, a detailed symptomatology of Krabbe disease became well established. In addition to demyelination and globoid cells, affected patients develop motor and cognitive disabilities. How these neurological disabilities originate is unknown. The discovery of neuronal α-synuclein inclusions in the brains of Krabbe patients provides a possible mechanism behind some of the observed symptoms, adding to the current proposed mechanisms of neurodegeneration [15–17]. The regional distribution of α-synuclein inclusions provide an interesting connection to some of the described neurological symptomatology.

Using the Twitcher mouse model, we were able to determine the regional and temporal distribution of α-synuclein inclusions. These inclusions were first observed in the pons and medulla of P10 Twitcher brains. The nuclei of the pons and medulla are major relay zones in the brain, playing a critical role in swallowing and emesis [52]. One of very first symptoms in infantile Krabbe disease is a growing difficulty in feeding, with impaired swallowing and vomiting [53]. Swallowing movements are primarily controlled by two groups of neurons in

the dorsal and ventrolateral medulla [54]. The medulla contains the center of emetic circuitry [55]. However, two areas of special note responsible for much of the emetic process are the lateral reticular formation, called the "vomiting center" of the medulla, coordinating somatic and visceral efferents responsible for vomiting [52] and the nucleus tractus solitaries, which produces outputs to the hypothalamus and the amygdala and receives vagus nerve inputs [55]. These areas are some of the first to show α-synuclein inclusions in the Twitcher.

Krabbe patients also undergo vision deterioration leading to blindness [56]. This has previously been attributed to atrophy of the optic nerve [57]. However, α-synuclein inclusions formed in the superior colliculus of P20 Twitcher brains, which then expanded to the hypothalamus at P30 and the lateral geniculate nucleus at P40. The temporal and regional distribution of these inclusions, affecting three subcortical structures that receive projections from the retina [58–60], suggests specific neuronal dysfunctions that may contribute to defects in Krabbe patients' vision.

One of the most striking deficits observed in Krabbe disease is the deterioration of motor movement, suggesting cerebellar degeneration. α-Synuclein has been shown to aggregate in the white matter and Purkinje cell axons of the cerebellum in patients with Parkinson's disease and dementia with Lewy bodies [61] and as well as in A30P transgenic mouse models of Parkinson's disease [62]. In Krabbe disease, the cerebellum undergoes atrophy without a compromise in cerebellar metabolic activity [63]. α-Synuclein inclusions were detected in the cerebellum as early as P20, coinciding with the onset of motor deficiencies in the mutant. Inclusions appeared to primarily affect the internal granular layer and later, the Purkinje and molecular layers. This progression may interfere with neuronal communication between the cerebellum and outer projections, compromising motor control. These neuronal defects likely contribute to the neurological symptoms and compound demyelination, magnifying the motor phenotype observed in mutant mice and affected patients.

The dorsal thalamus is the main relay area for all sensory and limbic pathways, sans olfaction, projecting to the cerebral cortex. Thalami of Parkinson's disease [64], GM1-gangliosidosis [65] and Sandhoff disease [66] patients contain abundant α-synuclein inclusions. While there is little experimental evidence showing thalamic components of Krabbe disease, two studies found hyperdensity of the thalamus when analyzed by CT scans [67,68]. Similarly, CT scans revealed increased densities in the caudate putamen of Krabbe patients [68]. Hypometabolism in the caudate of these patients [63] and of Parkinson's patients with severe motor dysfunction [69] has also been observed suggesting loss of cellular function. Likewise, α-synuclein inclusions in the caudate nucleus, the putamen and substantia nigra of Twitcher brains suggest that defects of the dopaminergic system may contribute to the impairment of motor movement and cognitive function in Krabbe disease.

α-Synuclein aggregation is a nucleation-dependent first-order process with a lag phase, an elongation phase and a steady-state phase [70,71]. Before the elongation phase begins a process called "seeding" occurs shortening the lag phase, and thus, increasing the rate of fibril formation [47]. During the elongation phase, α-synuclein exists in a soluble amyloid-like oligomeric phase before large insoluble filaments are formed. These oligomers, heterogeneous in structure [36,72,73], have been shown to form in vivo [74,75]. The toxic oligomer hypothesis states that oligomeric species are toxic forms causing neuronal dysfunction, while large fibrils are less toxic and possibly protective by sequestering toxic oligomers [36,39,76–78]. Protein formations resembling small oligomers, straight midsized fibrils, and larger fibril aggregates were detected in the Twitcher brain. Furthermore, psychosine was sufficient to induce a shortening of the lag phase, leading to the formation of large and abundant branched fibrils. These findings correlate with previous studies of both

in vitro and *in vivo* α-synuclein aggregation [39,76,79]. α-Synuclein binds synthetic and brain derived membranes [80–82] and oligomerizes in lipid droplets [83]. Lipid membrane binding is controversial, decreasing [84,85] or increasing aggregation [84]. α-Synuclein binds to lipid rafts and the A30P mutation decreased the protein levels in the synapse. Interestingly, blocking cholesterol or sphingolipid synthesis also depletes the levels of synaptic α-synuclein, suggesting that proper lipid raft architecture is essential for α-synuclein localization [86]. We have previously shown that psychosine accumulates in lipid rafts of the Twitcher mouse and Krabbe disease patients, disrupting architecture and function [4]. Thus, disruption of lipid raft architecture by psychosine in the Krabbe brain may affect α-synuclein localization to synapses, and increasing its aggregation in the neuronal cytoplasm as found in this study. Additionally, psychosine may alter α-synuclein conformation by direct binding to the protein (Santos and Bongarzone, Unpublished results). This pathogenic model may provide an alternative pathway for the mislocalization of α-synuclein from the presynaptic terminal, thereby affecting synaptic transmission and contributing to early synaptic dysfunction in Krabbe disease.

The discovery of α-synuclein neuronal inclusions is novel to Krabbe disease, granting consideration of Krabbe disease as a demyelinating synucleinopathy. Whether Krabbe disease shares some characteristics with MSA, a synucleinopathy with inclusions of α-synuclein in neurons and oligodendrocytes [87–89], needs further investigation Several questions remain to be studied, including whether or not these inclusions are true Lewy bodies, the mechanism regulating neuronal vulnerability in Krabbe disease and the spreading mechanism of α-synuclein inclusions throughout the Krabbe brain. The availability of a natural mouse model for this disease will facilitate exploration into these research areas.

Supplementary Material

Refer to Web version on PubMed Central for supplementary material.

Acknowledgments

References

1. Suzuki K, Iseki E, Togo T, et al. Neuronal and glial accumulation of alpha- and beta-synucleins in human lipidoses. Acta neuropathologica. 2007; 114:481–489. [PubMed: 17653558]

2. Wenger DA, Rafi MA, Luzi P. Molecular genetics of Krabbe disease (globoid cell leukodystrophy): diagnostic and clinical implications. Hum Mutat. 1997; 10:268–279. [PubMed: 9338580]

3. Igisu H, Suzuki K. Progressive accumulation of toxic metabolite in a genetic leukodystrophy. Science. 1984; 224:753–755. [PubMed: 6719111]

4. White AB, Givogri MI, Lopez-Rosas A, et al. Psychosine accumulates in membrane microdomains in the brain of krabbe patients, disrupting the raft architecture. J Neurosci. 2009; 29:6068–6077. [PubMed: 19439584]

5. Suzuki K. Twenty five years of the "psychosine hypothesis": a personal perspective of its history and present status. Neurochemical research. 1998; 23:251–259. [PubMed: 9482237]

6. Suzuki K, Suzuki Y. Krabbe's globoid cell leukodystrophy: deficiency of galactocerebroside beta-galactosidase activity. Journal of neuropathology and experimental neurology. 1971; 30:145.

7. Komiyama A, Suzuki K. Progressive impairment of Schwann cell proliferation in vitro in murine globoid cell leukodystrophy (twitcher). Brain Res. 1992; 598:1–9. [PubMed: 1486471]

8. Nagara H, Ogawa H, Sato Y, et al. The twitcher mouse: degeneration of oligodendrocytes in vitro. Brain Res. 1986; 391:79–84. [PubMed: 3513905]

9. Suzuki K, Suzuki K. Myelin pathology in the twitcher mouse. Ann N Y Acad Sci. 1990; 605:313–324. [PubMed: 2268119]

10. Tohyama J, Matsuda J, Suzuki K. Psychosine is as potent an inducer of cell death as C6-ceramide in cultured fibroblasts and in MOCH-1 cells. Neurochem Res. 2001; 26:667–671. [PubMed: 11519726]

11. Giri S, Jatana M, Rattan R, et al. Galactosylsphingosine (psychosine)-induced expression of cytokine-mediated inducible nitric oxide synthases via AP-1 and C/EBP: implications for Krabbe disease. Faseb J. 2002; 16:661–672. [PubMed: 11978730]

12. Giri S, Khan M, Nath N, et al. The role of AMPK in psychosine mediated effects on oligodendrocytes and astrocytes: Implication for Krabbe Disease. J Neurochem. 2008

13. Giri S, Khan M, Rattan R, et al. Krabbe disease: psychosine-mediated activation of phospholipase A2 in oligodendrocyte cell death. J Lipid Res. 2006; 47:1478–1492. [PubMed: 16645197]

14. Haq E, Giri S, Singh I, et al. Molecular mechanism of psychosine-induced cell death in human oligodendrocyte cell line. J Neurochem. 2003; 86:1428–1440. [PubMed: 12950451]

15. Cantuti Castelvetri L, Givogri MI, Hebert A, et al. The Sphingolipid Psychosine Inhibits Fast Axonal Transport in Krabbe Disease by Activation of GSK3beta and Deregulation of Molecular Motors. J Neurosci. 2013; 33:10048–10056. [PubMed: 23761900]

16. Cantuti-Castelvetri L, Zhu H, Givogri MI, et al. Psychosine induces the dephosphorylation of neurofilaments by deregulation of PP1 and PP2A phosphatases. Neurobiol Dis. 2012; 46:325–335. [PubMed: 22326830]

17. Castelvetri LC, Givogri MI, Zhu H, et al. Axonopathy is a compounding factor in the pathogenesis of Krabbe disease. Acta Neuropathol. 2011; 122:35–48. [PubMed: 21373782]

18. Dunn HG, Lake BD, Dolman CL, et al. THE NEUROPATHY OF KRABBE'S INFANTILE CEREBRAL SCLEROSIS: GLOBOID CELL LEUCODYSTROPHY. Brain. 1969; 92:329–344. [PubMed: 5790252]

19. Kurtz HJ, Fletcher TF. The peripheral neuropathy of canine globoid-cell leukodystrophy (krabbe-type). Acta Neuropathol. 1970; 16:226–232. [PubMed: 5478211]

20. Krabbe K. A new familial, infantile form of diffuse brain sclerosis. Brain. 1916; 39:74–114.

21. Smith B, Galbiati F, Castelvetri LC, et al. Peripheral neuropathy in the Twitcher mouse involves the activation of axonal caspase 3. ASN Neuro. 2011; 3:213–222.

22. Duchen LW, Eicher EM, Jacobs JM, et al. Hereditary leucodystrophy in the mouse: the new mutant twitcher. Brain. 1980; 103:695–710. [PubMed: 7417782]

23. Sakai N, Inui K, Tatsumi N, et al. Molecular cloning and expression of cDNA for murine galactocerebrosidase and mutation analysis of the twitcher mouse, a model of Krabbe's disease. J Neurochem. 1996; 66:1118–1124. [PubMed: 8769874]

24. Kobayashi T, Yamanaka T, Jacobs JM, et al. The Twitcher mouse: an enzymatically authentic model of human globoid cell leukodystrophy (Krabbe disease). Brain Res. 1980; 202:479–483. [PubMed: 7437911]

25. Jakes R, Spillantini MG, Goedert M. Identification of two distinct synucleins from human brain. FEBS letters. 1994; 345:27–32. [PubMed: 8194594]

26. Withers GS, George JM, Banker GA, et al. Delayed localization of synelfin (synuclein, NACP) to presynaptic terminals in cultured rat hippocampal neurons. Brain Res Dev Brain Res. 1997; 99:87–94.

27. Byrne EJ, Lennox G, Lowe J, et al. Diffuse Lewy body disease: clinical features in 15 cases. Journal of neurology, neurosurgery, and psychiatry. 1989; 52:709–717.

28. Hurtig HI, Trojanowski JQ, Galvin J, et al. Alpha-synuclein cortical Lewy bodies correlate with dementia in Parkinson's disease. Neurology. 2000; 54:1916–1921. [PubMed: 10822429]

29. Lennox G, Lowe J, Byrne EJ, et al. Diffuse Lewy body disease. Lancet. 1989; 1:323–324. [PubMed: 2563473]

30. Lennox G, Lowe J, Landon M, et al. Diffuse Lewy body disease: correlative neuropathology using anti-ubiquitin immunocytochemistry. Journal of neurology, neurosurgery, and psychiatry. 1989; 52:1236–1247.

31. Lippa CF, Fujiwara H, Mann DM, et al. Lewy bodies contain altered alpha-synuclein in brains of many familial Alzheimer's disease patients with mutations in presenilin and amyloid precursor protein genes. The American journal of pathology. 1998; 153:1365–1370. [PubMed: 9811326]

32. Spillantini MG, Schmidt ML, Lee VM, et al. Alpha-synuclein in Lewy bodies. Nature. 1997; 388:839–840. [PubMed: 9278044]

33. Hashimoto M, Hsu LJ, Sisk A, et al. Human recombinant NACP/alpha-synuclein is aggregated and fibrillated in vitro: relevance for Lewy body disease. Brain research. 1998; 799:301–306. [PubMed: 9675319]

34. Biere AL, Wood SJ, Wypych J, et al. Parkinson's disease-associated alpha-synuclein is more fibrillogenic than beta- and gamma-synuclein and cannot cross-seed its homologs. The Journal of biological chemistry. 2000; 275:34574–34579. [PubMed: 10942772]

35. Kessler JC, Rochet JC, Lansbury PT Jr. The N-terminal repeat domain of alpha-synuclein inhibits beta-sheet and amyloid fibril formation. Biochemistry. 2003; 42:672–678. [PubMed: 12534279]

36. Conway KA, Lee SJ, Rochet JC, et al. Acceleration of oligomerization, not fibrillization, is a shared property of both alpha-synuclein mutations linked to early-onset Parkinson's disease: implications for pathogenesis and therapy. Proceedings of the National Academy of Sciences of the United States of America. 2000; 97:571–576. [PubMed: 10639120]

37. Goldberg MS, Lansbury PT Jr. Is there a cause-and-effect relationship between alpha-synuclein fibrillization and Parkinson's disease? Nature cell biology. 2000; 2:E115–119.

38. Cabin DE, Shimazu K, Murphy D, et al. Synaptic vesicle depletion correlates with attenuated synaptic responses to prolonged repetitive stimulation in mice lacking alpha-synuclein. The Journal of neuroscience : the official journal of the Society for Neuroscience. 2002; 22:8797–8807. [PubMed: 12388586]

39. Gadad BS, Britton GB, Rao KS. Targeting oligomers in neurodegenerative disorders: lessons from alpha-synuclein, tau, and amyloid-beta peptide. J Alzheimers Dis. 2011; 24 (Suppl 2):223–232. [PubMed: 21460436]

40. Waxman EA, Giasson BI. Molecular mechanisms of alpha-synuclein neurodegeneration. Biochimica et biophysica acta. 2009; 1792:616–624. [PubMed: 18955133]

41. Giasson BI, Murray IV, Trojanowski JQ, et al. A hydrophobic stretch of 12 amino acid residues in the middle of alpha-synuclein is essential for filament assembly. The Journal of biological chemistry. 2001; 276:2380–2386. [PubMed: 11060312]

42. Giasson BI, Uryu K, Trojanowski JQ, et al. Mutant and wild type human alpha-synucleins assemble into elongated filaments with distinct morphologies in vitro. The Journal of biological chemistry. 1999; 274:7619–7622. [PubMed: 10075647]

43. Miake H, Mizusawa H, Iwatsubo T, et al. Biochemical characterization of the core structure of alpha-synuclein filaments. The Journal of biological chemistry. 2002; 277:19213–19219. [PubMed: 11893734]

44. Murray IV, Giasson BI, Quinn SM, et al. Role of alpha-synuclein carboxy-terminus on fibril formation in vitro. Biochemistry. 2003; 42:8530–8540. [PubMed: 12859200]

45. Narhi L, Wood SJ, Steavenson S, et al. Both familial Parkinson's disease mutations accelerate alpha-synuclein aggregation. The Journal of biological chemistry. 1999; 274:9843–9846. [PubMed: 10092675]

46. Serpell LC, Berriman J, Jakes R, et al. Fiber diffraction of synthetic alpha-synuclein filaments shows amyloid-like cross-beta conformation. Proceedings of the National Academy of Sciences of the United States of America. 2000; 97:4897–4902. [PubMed: 10781096]

47. Wood SJ, Wypych J, Steavenson S, et al. alpha-synuclein fibrillogenesis is nucleation-dependent. Implications for the pathogenesis of Parkinson's disease. The Journal of biological chemistry. 1999; 274:19509–19512. [PubMed: 10391881]

48. Galbiati F, Basso V, Cantuti L, et al. Autonomic denervation of lymphoid organs leads to epigenetic immune atrophy in a mouse model of Krabbe disease. J Neurosci. 2007; 27:13730–13738. [PubMed: 18077684]

49. Youmans KL, Tai LM, Nwabuisi-Heath E, et al. APOE4-specific changes in Abeta accumulation in a new transgenic mouse model of Alzheimer disease. J Biol Chem. 2012; 287:41774–41786. [PubMed: 23060451]

50. Sharon R, Bar-Joseph I, Frosch MP, et al. The formation of highly soluble oligomers of alpha-synuclein is regulated by fatty acids and enhanced in Parkinson's disease. Neuron. 2003; 37:583–595. [PubMed: 12597857]

51. Cleary JP, Walsh DM, Hofmeister JJ, et al. Natural oligomers of the amyloid-beta protein specifically disrupt cognitive function. Nat Neurosci. 2005; 8:79–84. [PubMed: 15608634]

52. Barnes JH. The physiology and pharmacology of emesis. Mol Aspects Med. 1984; 7:397–508. [PubMed: 6151112]

53. Noronha LD, Sampaio G, Bruck I, et al. Krabbe s disease - case report. J Pediatr (Rio J). 2000; 76:79–82. [PubMed: 14647705]

54. Jean A. Brain stem control of swallowing: neuronal network and cellular mechanisms. Physiological reviews. 2001; 81:929–969. [PubMed: 11274347]

55. Hornby PJ. Central neurocircuitry associated with emesis. Am J Med. 2001; 111(Suppl 8A):106S–112S. [PubMed: 11749934]

56. Hagberg B. Krabbe's disease: clinical presentation of neurological variants. Neuropediatrics. 1984; 15 (Suppl):11–15. [PubMed: 6546163]

57. Crome L, Hanefeld F, Patrick D, et al. Late onset globoid cell leucodystrophy. Brain : a journal of neurology. 1973; 96:841–848. [PubMed: 4773865]

58. Altman J, Carpenter MB. Fiber projections of the superior colliculus in the cat. The Journal of comparative neurology. 1961; 116:157–177. [PubMed: 13682733]

59. Trachtman JN. Vision and the hypothalamus. Optometry. 2010; 81:100–115. [PubMed: 20152784]

60. Harrington ME. The ventral lateral geniculate nucleus and the intergeniculate leaflet: interrelated structures in the visual and circadian systems. Neurosci Biobehav Rev. 1997; 21:705–727. [PubMed: 9353800]

61. Mori F, Piao YS, Hayashi S, et al. Alpha-synuclein accumulates in Purkinje cells in Lewy body disease but not in multiple system atrophy. Journal of neuropathology and experimental neurology. 2003; 62:812–819. [PubMed: 14503637]

62. Lotharius J, Brundin P. Pathogenesis of Parkinson's disease: dopamine, vesicles and alpha-synuclein. Nature reviews Neuroscience. 2002; 3:932–942.

63. Al-Essa MA, Bakheet SM, Patay ZJ, et al. Clinical and cerebral FDG PET scan in a patient with Krabbe's disease. Pediatric neurology. 2000; 22:44–47. [PubMed: 10669205]

64. Rub U, Del Tredici K, Schultz C, et al. Parkinson's disease: the thalamic components of the limbic loop are severely impaired by alpha-synuclein immunopositive inclusion body pathology. Neurobiology of aging. 2002; 23:245–254. [PubMed: 11804710]

65. Kobayashi O, Takashima S. Thalamic hyperdensity on CT in infantile GM1-gangliosidosis. Brain & development. 1994; 16:472–474. [PubMed: 7694998]

66. Stalker HP, Han BK. Thalamic hyperdensity: a previously unreported sign of Sandhoff disease. AJNR Am J Neuroradiol. 1989; 10:S82. [PubMed: 2505588]

67. Jardim LB, Giugliani R, Fensom AH. Thalamic and basal ganglia hyperdensities--a CT marker for globoid cell leukodystrophy? Neuropediatrics. 1992; 23:30–31. [PubMed: 1565214]

68. Kwan E, Drace J, Enzmann D. Specific CT findings in Krabbe disease. AJR Am J Roentgenol. 1984; 143:665–670. [PubMed: 6331756]

69. Eidelberg D, Takikawa S, Moeller JR, et al. Striatal hypometabolism distinguishes striatonigral degeneration from Parkinson's disease. Annals of neurology. 1993; 33:518–527. [PubMed: 8498828]

70. Lundvig D, Lindersson E, Jensen PH. Pathogenic effects of alpha-synuclein aggregation. Brain research Molecular brain research. 2005; 134:3–17. [PubMed: 15790525]

71. Harper JD, Lansbury PT Jr. Models of amyloid seeding in Alzheimer's disease and scrapie: mechanistic truths and physiological consequences of the time-dependent solubility of amyloid proteins. Annual review of biochemistry. 1997; 66:385–407.

72. Volles MJ, Lee SJ, Rochet JC, et al. Vesicle permeabilization by protofibrillar alpha-synuclein: implications for the pathogenesis and treatment of Parkinson's disease. Biochemistry. 2001; 40:7812–7819. [PubMed: 11425308]

73. Conway KA, Harper JD, Lansbury PT. Accelerated in vitro fibril formation by a mutant alpha-synuclein linked to early-onset Parkinson disease. Nature medicine. 1998; 4:1318–1320.

74. Dickson DW, Liu W, Hardy J, et al. Widespread alterations of alpha-synuclein in multiple system atrophy. The American journal of pathology. 1999; 155:1241–1251. [PubMed: 10514406]

75. Kahle PJ, Neumann M, Ozmen L, et al. Selective insolubility of alpha-synuclein in human Lewy body diseases is recapitulated in a transgenic mouse model. The American journal of pathology. 2001; 159:2215–2225. [PubMed: 11733371]

76. Winner B, Jappelli R, Maji SK, et al. In vivo demonstration that alpha-synuclein oligomers are toxic. Proceedings of the National Academy of Sciences of the United States of America. 2011; 108:4194–4199. [PubMed: 21325059]

77. Pountney DL, Voelcker NH, Gai WP. Annular alpha-synuclein oligomers are potentially toxic agents in alpha-synucleinopathy. Hypothesis Neurotoxicity research. 2005; 7:59–67.

78. Rochet JC, Conway KA, Lansbury PT Jr. Inhibition of fibrillization and accumulation of prefibrillar oligomers in mixtures of human and mouse alpha-synuclein. Biochemistry. 2000; 39:10619–10626. [PubMed: 10978144]

79. Conway KA, Lee SJ, Rochet JC, et al. Accelerated oligomerization by Parkinson's disease linked alpha-synuclein mutants. Annals of the New York Academy of Sciences. 2000; 920:42–45. [PubMed: 11193175]

80. Eliezer D, Kutluay E, Bussell R Jr, et al. Conformational properties of alpha-synuclein in its free and lipid-associated states. Journal of molecular biology. 2001; 307:1061–1073. [PubMed: 11286556]

81. Jo E, McLaurin J, Yip CM, et al. alpha-Synuclein membrane interactions and lipid specificity. The Journal of biological chemistry. 2000; 275:34328–34334. [PubMed: 10915790]

82. Ding TT, Lee SJ, Rochet JC, et al. Annular alpha-synuclein protofibrils are produced when spherical protofibrils are incubated in solution or bound to brain-derived membranes. Biochemistry. 2002; 41:10209–10217. [PubMed: 12162735]

83. Sharon R, Goldberg MS, Bar-Josef I, et al. alpha-Synuclein occurs in lipid-rich high molecular weight complexes, binds fatty acids, and shows homology to the fatty acid-binding proteins. Proceedings of the National Academy of Sciences of the United States of America. 2001; 98:9110–9115. [PubMed: 11481478]

84. Narayanan V, Scarlata S. Membrane binding and self-association of alpha-synucleins. Biochemistry. 2001; 40:9927–9934. [PubMed: 11502187]

85. Zhu M, Fink AL. Lipid binding inhibits alpha-synuclein fibril formation. The Journal of biological chemistry. 2003; 278:16873–16877. [PubMed: 12621030]

86. Fortin DL, Troyer MD, Nakamura K, et al. Lipid rafts mediate the synaptic localization of alpha-synuclein. The Journal of neuroscience : the official journal of the Society for Neuroscience. 2004; 24:6715–6723. [PubMed: 15282274]

87. Ahmed Z, Asi YT, Sailer A, et al. The neuropathology, pathophysiology and genetics of multiple system atrophy. Neuropathol Appl Neurobiol. 2012; 38:4–24. [PubMed: 22074330]

88. Matsuo A, Akiguchi I, Lee GC, et al. Myelin degeneration in multiple system atrophy detected by unique antibodies. Am J Pathol. 1998; 153:735–744. [PubMed: 9736024]

89. Wakabayashi K, Takahashi H. Cellular pathology in multiple system atrophy. Neuropathology. 2006; 26:338–345. [PubMed: 16961071]
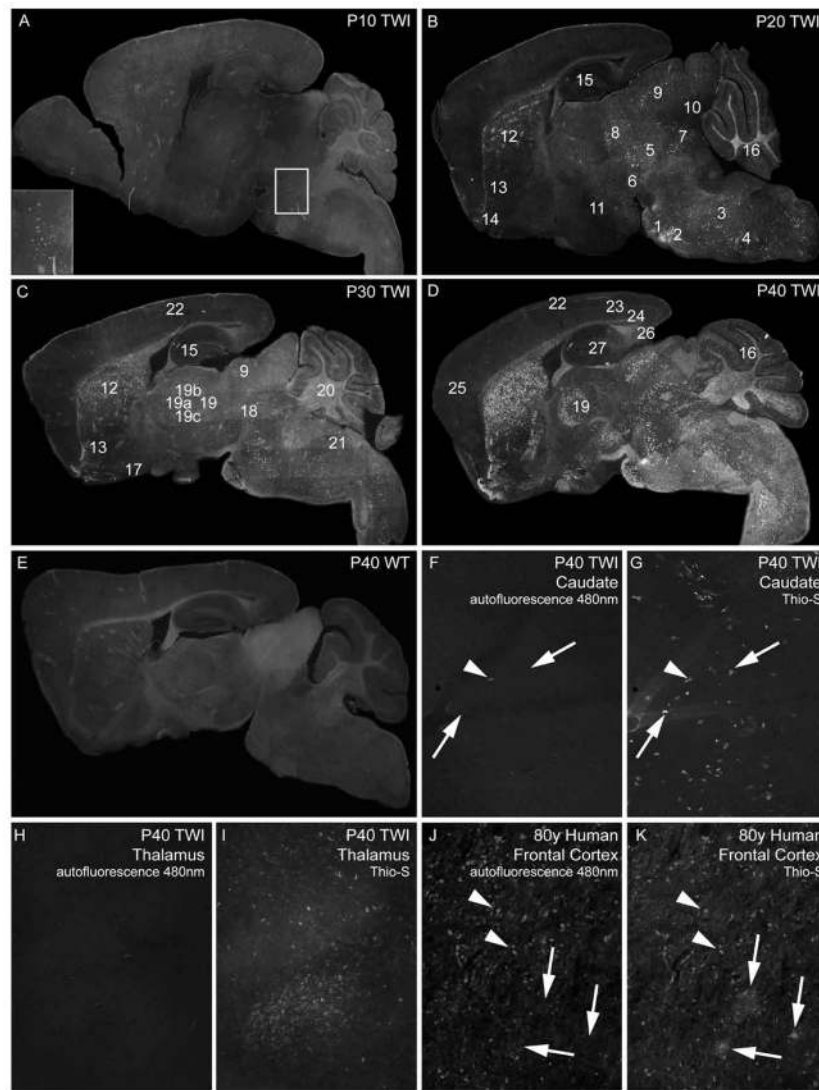
Figure 1. Distribution of Thioflavin-S reactive material in the Twitcher brain
A–E) Composite mapping of thioflavin-S (Thio-S) reactive deposits at 10 (A), 20 (B), 30 (C) and 40 (D) days of age in the Twitcher (TWI) brain. E shows the composite image of thioflavin-S staining of a 40 day-old wild type (WT) brain. Insert in A marks the pontine region (pons). 1, pontine grey area; 2, superior olivary complex; 3, medulla; 4, spinal nucleus of the trigeminal nerve; 5, midbrain; 6, substantia nigra; 7, reticular nucleus; 8, dorsal lateral geniculate nucleus; 9, superior colliculus; 10, inferior colliculus; 11, hypothalamus; 12, caudate putamen; 13, nucleus accumbens; 14, olfactory tubercle; 15, hippocampus; 16, cerebellar internal granular layer; 17, hypothalamic pre-optic area; 18, superior red nucleus; 19, thalamus; 19a, lateral dorsal nucleus; 19b, anteroventral nucleus; 19c, reticular nucleus; 20, cerebellar arbor vitae; 21, vestibular nuclei; 22, cortex layer 1; 23, cortex layers 3 and 4; 24, cortex layer 6b; 25, frontal cortex; 26, subiculum and 27, dentate gyrus. Composite images were taken using a 5× objective and each contain 60–70 individual images. **F–K)** Unstained (F, H) and thioflavin-S stained (G, H) TWI caudate and thalamus tissue imaged under 480nm filter. Scarce autofluorescent material (arrowhead) seen in TWI compared to abundant thioflavin-S reactive inclusions (arrows). Positive control of autofluorescent lipofucsin accumulations (arrowheads) compared to thioflavin-S reactive

deposits (arrows) shown in aged human frontal cortex (J, K). Images in (F–K) taken with 10× objective.
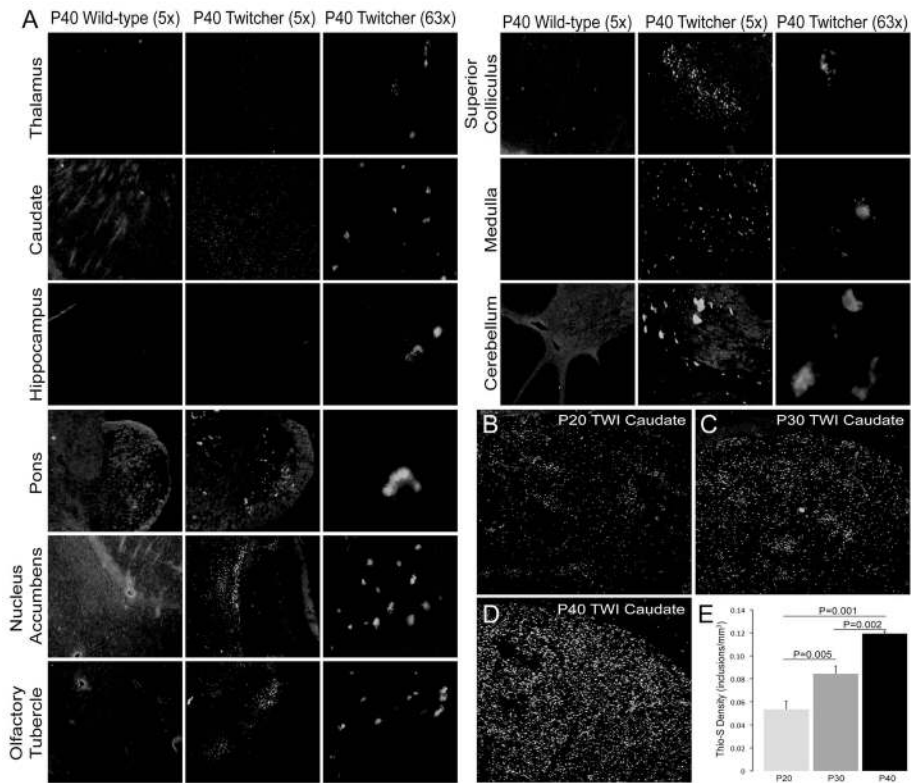
Figure 2. Regional distribution of thioflavin-S deposits and stereological quantification of thioflavin-S reactive deposits during postnatal development of the Twitcher caudate putamen
A) Magnified (5× and 63×) images of thioflavin-S reactive inclusions in multiple anatomical regions of the P40 Twitcher (TWI) and P40 wild type (WT) brain regions. **B–D)** Confocal microscopy shows increasing abundance of thioflavin-S reactive inclusions in the Twitcher caudate putamen at 20 (B), 30 (C) and 40 (D) days of age. **E)** Stereological quantification of the density of thioflavin-S (thio-S) deposits (inclusions/mm^3) shows significant (ANOVA) increases in inclusion density at each time point. Data is expressed as the mean +/− SEM of 3 mice per time point.
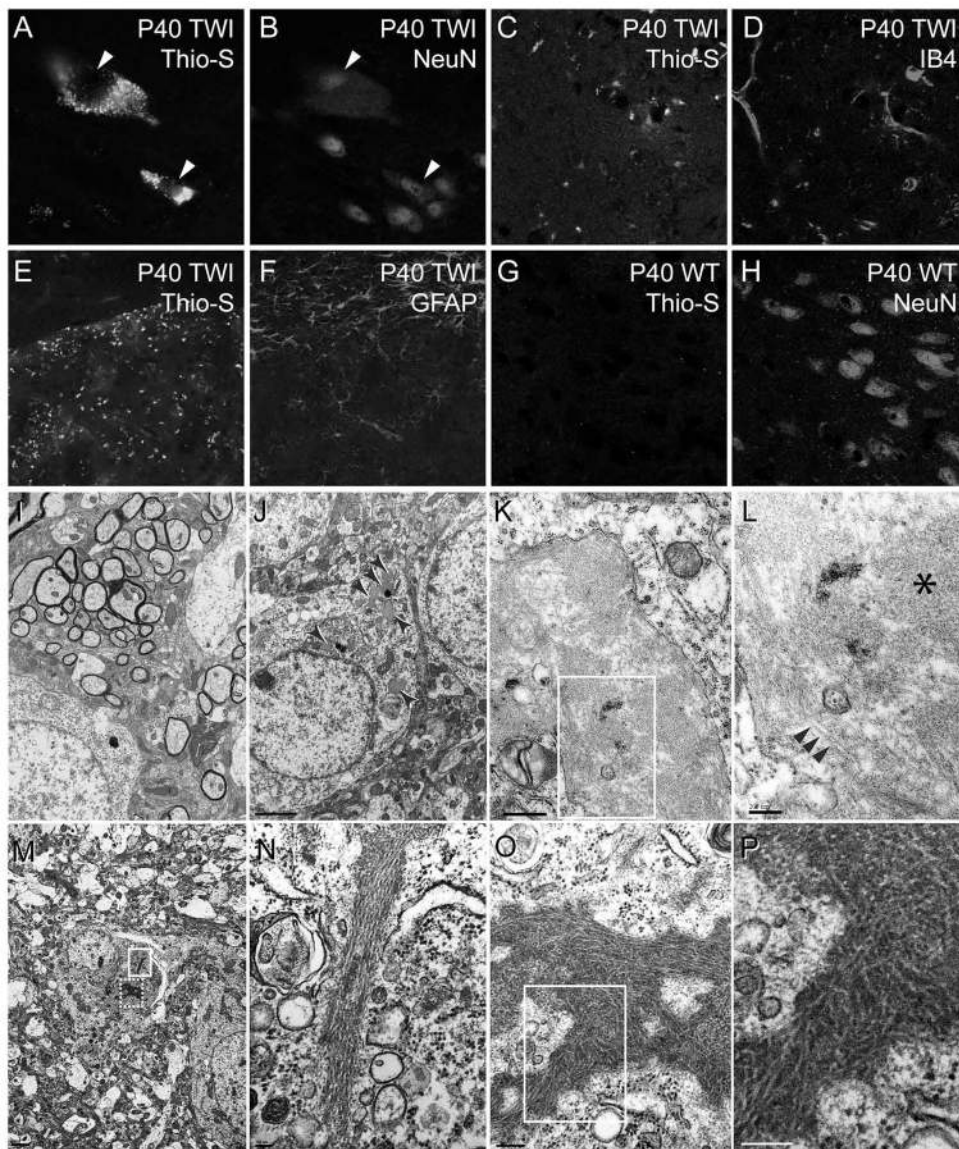
Figure 3. Thioflavin-S material is primarily localized in neurons
A–D) Sections of P30 Twitcher brain were doubly stained for thioflavin-S (thio-S) (A, C) and the neuronal antigen NeuN (B) and the microglial lectin IB4 (D). **E–H)** Confocal imaging confirmed the absence of Thio-S staining in twitcher GFAP positive astrocytes (E, F) and wild-type (WT) neurons (G, H). All images were collected using a 63× objective. **I–P)** Electron microscopy analysis performed on ultrathin sections of P40 Twitcher caudate putamen showed pathological inclusions only in Twitcher (arrowheads in J) but not in wild-type neurons (I). A stereotypical inclusion (K) is magnified in L (boxed area) showing the presence of globular (asterisk in L) and fibrillized material (arrowheads in L). Other neuronal inclusions consist of stereotypic assemblies of fibrillized material (M). Two of these inclusions (boxed areas in M) are shown in higher magnification in N-P. These inclusions consist of long tubular, typically straight, fibrils of approximately 100–150nm in width, and can be up to 1.5μm in length. Scale bars: I, J, 2μm; K, 500nm; L, 200nm; M, 1μm; N, 100nm; O, 200nm; P, 100nm.
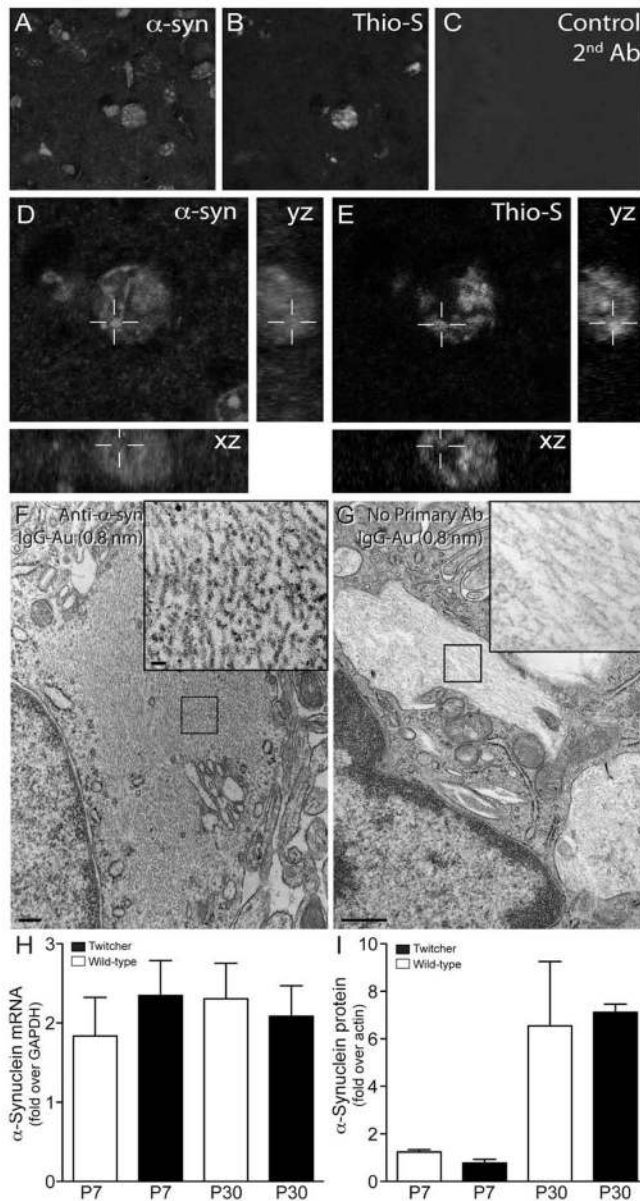
Figure 4. Thioflavin-S reactive inclusions contain α-synuclein

A–E) Sections of P30 Twitcher brain were doubly stained with a monoclonal antibody to α-synuclein (A, D) and thioflavin-S (B, D). Sections were scanned using confocal microscopy and orthogonal yz, xz reconstructions rendered using ImageJ software (NIH). α-synuclein was detected to be predominantly associated with thioflavin-S reactive inclusions. **F, G)** Free floating sections of mutant caudate were immunostained for α-synuclein and processed for immunoelectron microscopy using secondary antibodies conjugated with 0.8 nm gold particles. Inclusions in mutant neurons (F, inset) showed positive immunoreaction. Control of non-specific binding using secondary-Au antibodies showed no reaction (G, inset). **H, I)** Analyses for mRNA (H) and protein (I) levels of α-synuclein were done by RT-PCR and immunoblotting using P7 and P30 Twitcher and WT brain. Immunoblotting was performed with antibodies recognizing actin and monomeric forms α-synuclein. Detectable bands representing α-synuclein where quantified as the fold increase over actin using ImageJ

software (NIH). Levels of α-synuclein mRNA and protein were not significantly different between Twitcher and WT at either time point.
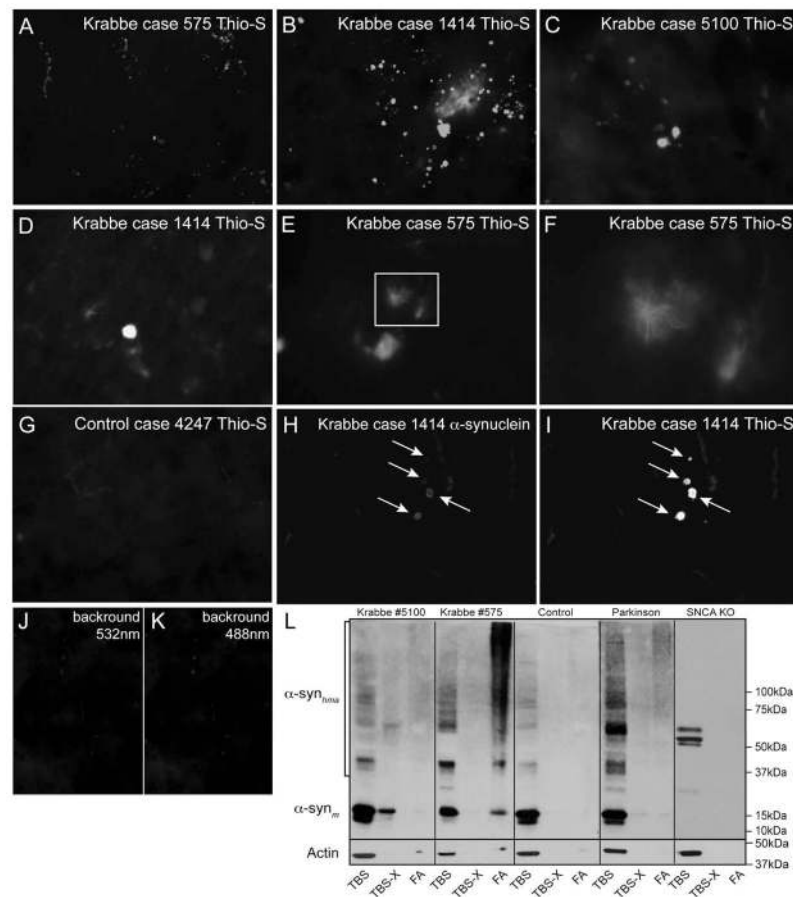
Figure 5. Thioflavin-S reactive inclusions of aggregated α-synuclein are present in the brain of Krabbe human patients

A–G) Autopsied frontal cortex samples from three human cases of infantile Krabbe disease were obtained and processed for thioflavin-S staining. All three cases of infantile Krabbe disease were affected by abundant thioflavin-S reactive deposits, which were primarily located in the cortical grey matter. Most inclusions appeared as an amorphous material (D) but others showed a core of dense thioflavin-S positive material decorated with filamentous fibrils irradiating from the core center (inset in E magnified in F). Sections from age-matching control human brains were devoid of thioflavin-S reactive material (G). **H–K)** Double immunohistochemistry detected the presence of aggregated α-synuclein (I) in most thioflavin-S inclusions (H). Images in J, K are controls of background fluorescence and show non-specific fluorescence originating from blood cells in brain vessels. Images in A–C and G–K were collected using a 40× objective. Images in D–F were collected using a 63× objective. **L)** SDS-PAGE separations of TBS, TBS-triton-X (TBS-X) and formic acid (FA) protein extracts from age-matching control and infantile Krabbe basal ganglia were immunoblotted with monoclonal antibodies against epitopes in monomeric α-synuclein. Monomeric α-synuclein (~15kDa) was present only in the TBS and some TBS-X fractions. An increased amount of high molecular weight aggregates of α-synuclein (α-syn$_{hma}$) were visible in the Krabbe samples for all fractions. A sample of frontal cortex from a Parkinson's disease case was included as a positive control showing levels of high molecular weight α-synuclein similar to the amount seen in Krabbe tissue. Whole cell brain lysate from a one month-old SNCA KO mouse was also included which showed no detectable monomeric α-synuclein and only a few additional non-specific bands.
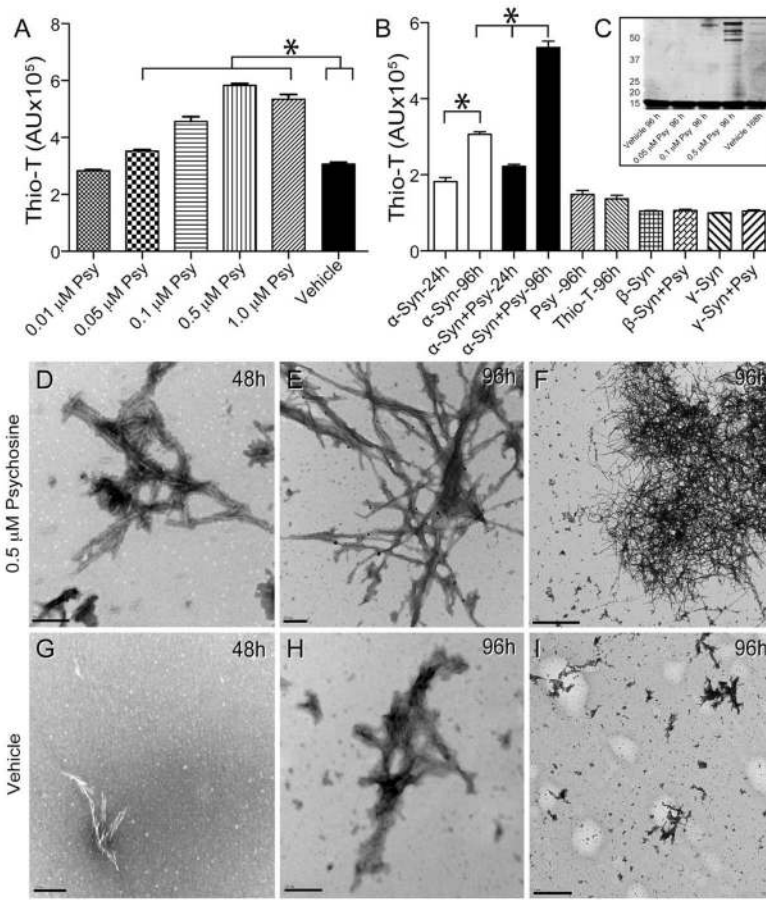
Figure 6. Psychosine increases the rate of α-synuclein fibrillation
A, B) An in vitro fibrillization assay was performed by incubating recombinant human α-synuclein (α-syn) in the presence of increasing concentrations of psychosine (Psy) or vehicle (0.005% ethanol/PBS) and measuring emitted fluorescence from thioflavin-T (thio-T) for up to 96h. Significant (ANOVA, $p < 0.05$) increases of thioflavin-T fluorescence were measured in the presence of psychosine in a dose dependent manner. Psychosine alone did not show fluorescence above background levels from thioflavin-T. Psychosine did not cause fibrillization of either β- or γ-synucleins. **C)** Aliquots of fibrillized α-synuclein in the presence or absence of different concentrations of psychosine were analyzed by gel separation. Protein bands were developed using Sypro fluorescent stain and scanned using a Typhoon fluorometer. **D–I)** Transmission electron microscopy detected the presence of abundant fibrillized α-synuclein in the presence of 0.5 μM psychosine 48 hours after treatment (D). Fibrillization of α-synuclein was more abundant at 96 h of incubation in the presence of psychosine (E, F). α-Synuclein formed straight groups of filaments approximately 50–75nm in width and also formed larger, branched aggregates approximately 300–700 nm in length (E, F). Smaller and less abundant α-synuclein fibrils were detected in vehicle-treated conditions (G–I). Scale bars: D, E, G, H, 200 nm; F, 2μm; I, 1μm.

Table I

Distribution of Psychosine in the Twitcher brain

Area	Psychosine (pmol/mg protein)	
	Twitcher	Wild-Type
Cortex		
Frontal	31.6±6.3[*]	<1
Olfactory	42.8±11.3[*]	<1
Parietal	32.8±4.5[*]	<1
Enthorinal	29.3±2.9[*]	<1
Thalamus	289.2±15.7[*]	<1
Brainstem	440.2±52.2[*]	<1
Hippocampus		
Anterior	65±17.9[*]	<1
Posterior	107.9±29.3[*]	<1
Cerebellum	150.2±28.3[*]	<1

[*] ANOVA significant $p<0.0001$